8-10-2005

Development of a Laminar Construction Quadrupole Ion Trap

Nagalakshmi Tentu
University of New Orleans

DEVELOPMENT OF A LAMINAR CONSTRUCTION QUADRUPOLE ION TRAP

A Thesis

Submitted to the Graduate Faculty of the
University of New Orleans
in partial fulfillment of the
requirements for the degree of

Master of Science
in
The Department of Chemistry

by

Nagalakshmi Tentu

B.Pharmacy, Osmania University, India, 2002

August, 2005

To my Parents, for their love and support

ACKNOWLEDGEMENTS

I would like to express my heartfelt gratitude to my research advisor Dr. Kevin J. Boyd for his valuable guidance, encouragement and support throughout my graduate studies at UNO.

I would like to thank Dr. Carl Ventrice from the Physics department and Harry Rees from the Electronics shop for their help and advices. I also thank Dr. Edwin D. Stevens, Professor and Chair of the Department of Chemistry and Dr. Steven W. Rick, Asst. Professor for being on my thesis committee.

I wish to express my gratitude to my husband Srinu and my brother Chinni for their constant support throughout.

Last, but not least, I am deeply grateful to my parents for their sacrifices, blessings and moral support.

TABLE OF CONTENTS

LIST OF FIGURES

LIST OF GRAPHS

ABSTRACT

The three-dimensional quadrupole ion trap (QIT) is an extraordinary device. It functions both as an ion store in which gaseous ions can be confined for a period of time and as a mass spectrometer of considerable mass range and variable mass resolution. Over the past few decades, it has evolved into a powerful tool for both research and routine analysis. The basic objective of this thesis is the development of a three-dimensional quadrupole ion trap with cylindrical symmetry in laminar approximation. The laminar construction allows hyperbolic geometry to be well approximated with minimal construction effort and also provides more access into the trap through interlaminar spaces without disruption of the field. The performance of the trap is examined in the mass selective trapping mode and mass-selective instability mode. Fourier detection is also done. Resolution of our instrument is limited by the external hardware. There is not good enough data quality and so not a good enough spectrum to predict its resolution accurately. A few changes to the instrumentation of the trap will improve the resolution.

CHAPTER 1

INTRODUCTION

1.1. Introduction

The quadrupole ion trap (QIT) belongs to the dynamic type of mass analyzers in which the ion trajectories are influenced by a set of time-dependent forces [1]. It is based on the principle that ions can be trapped in a symmetrical three-dimensional electric radiofrequency field under appropriate conditions. This is achieved when appropriate electric potentials are applied to electrodes that have a hyperbolic geometric form [2]. In a quadrupole electric field, the force on a charged particle is linearly proportional to its displacement from the origin. Ions of appropriate mass-to-charge ratios are trapped in the time-dependent potential energy well created by the field.

The ion trap originated from the pioneering work of Paul and Steinwedel, who were awarded Nobel Prize for Physics in 1989 for this discovery [3]. For over three decades, many research groups are engaged in instrumental development and applications of the ion trap.

The QIT is the three-dimensional analogue of the linear quadrupole mass filter [4]. It can be used as a mass analyzer because of the control available over the stability of the ion motion in an electric field. It is a sensitive and versatile mass spectrometer. It has the ability to perform multiple stages of mass spectrometry. With the increasing number of uses, QIT is now considered as a

standard instrument for mass spectrometry.

1.2 Research Objective

The main objective of this thesis is to develop and characterize the performance of a three-dimensional quadrupole ion trap using the laminar approximation.

1.3 Contribution of Thesis

A quadrupole ion trap is constructed according to the laminar approximation. Its performance is characterized by operating the trap in two different modes and the mass spectra of the background gases present inside the chamber are obtained. Fourier detection of the ion signal is also done. This thesis introduces the various features and advantages of the laminar approximated quadrupole ion trap.

1.4 Organization of Thesis

Chapter 2 describes the theory of the quadrupole ion trap. It discusses the potential well inside a quadrupole ion trap, the Mathieu stability diagram and the ion's trajectories inside the potential well of the trap. It also mentions the advantages of the laminar-constructed quadrupole ion trap over the conventional quadrupole ion trap. Chapter 3 gives the details of the experimental setup. It describes the vacuum system, RF generator, channeltron detector and the homemade ion source used in the experiments. Chapter 4 gives the experimental

results obtained during the thesis research. It discusses the results obtained in two different modes of operation of the laminar constructed quadrupole ion trap. Chapter 5 deals with the Fourier detection of the ion signal. It introduces the concept of the Fourier transform and describes the low-pass filter, pulsing circuit and the differential amplifier constructed for Fourier detection. It also gives the spectra obtained by Fourier detection. Finally Chapter 6 concludes the report by discussing the results presented in Chapter 4 & 5. It also discusses the limitations and the improvements that can be made to improve the resolution of the instrument.

CHAPTER 2

THEORY OF THE QUADRUPOLE ION TRAP

2.1 Introduction to the theory

As implied by its name, the ion trap operates on the basis of first storing the ions and then facilitating their detection according to their mass/charge (m/z) ratio by varying the stability of the ion's trajectory [4]. The confining capacity of the trap is due to the formation of a trapping potential well when appropriate potentials are applied to the electrodes. According to the laws of electrodynamics, the potential distribution inside the enclosed volume of an ion trap is determined by the potential along the enclosing border surfaces [5]. Neglecting the tiny potential drops caused by the resistance effect of possible surface currents and the possible charge-up effects of unclean surfaces, metal electrodes have the same electrical potential over the entire surface, thus showing equipotential surfaces. By knowing the exact shape of the equipotential surfaces embracing the cell volume desired, metal electrodes of exact shape are produced using numerically controlled lathes and mills. When correct voltages are applied to correctly positioned electrodes, the desired potential distribution is obtained inside the ion trap. Boundary conditions are imposed by the geometric structure of the electrodes, which are assumed to be equipotential surfaces, and by the static and rf voltages applied to each of them.

In general, the electric field inside the trap is determined from the Maxwell's equations using appropriate boundary conditions [5]. The effective potential well is created in three dimensions by a linear combination of quasipotentials. Consider a particle of charge q and mass m moving in an external electric field E(r, t). Let us assume that the quasistationary electric field E(r, t) is composed of a static field, $E_s(r)$, and a time-dependent part, $E_0(r) \cos(\Omega t + \delta)$, where $E_0(r)$ is the field amplitude, $\Omega = 2\pi f$ is a fixed angular frequency, and δ is a phase. In this case both the static $E_s(r)$ and the time-varying part of the field, $E_{rf} = E_0(r) \cos \Omega t$, can be derived from the potentials ϕ_s and ϕ_{rf}, respectively. Because of the superposition principle, $\phi = \phi_s + \phi_{rf}$ and the potential, ϕ, is reduced to the solution of Laplace's equation under the inclusion of the appropriate boundary conditions and the space charge, $\rho(r)$, which is given by:

$$\nabla^2 \phi(\vec{r}) = -4\pi\rho(\vec{r})$$

The general solution (effective potential) of Laplace's equation for any 2n-pole is obtained by setting $\phi(r = r_0, \varphi) = \phi_0 \cos n\varphi$ and $\phi\ (r = r_0, \varphi) = 0$ and by using the reduced variable $\vec{r} = r/r_0$ as

$$\phi(r, \varphi) = \phi_0 \vec{r}^{\,n} \cos n\varphi$$

By the application of the Laplace condition that the rate of change of field

gradient should be uniform throughout the trap volume, in the space-charge-free limit, Laplace's equation becomes simply:

$$\nabla^2 \phi(\vec{r}) = 0$$

Since there is no change in the field gradient, let it be equal to a constant k. Then

$$\phi_0 \vec{r}^{\,n} \cos n\varphi = k \,,$$

and

$$\vec{r}^{\,n} \cos n\varphi = \frac{k}{\phi_0} .$$

For a quadrupole, where n = 2, the above equation becomes:

$$r^2 \cos 2\varphi = \text{constant } (k^2).$$

Then using the trigonometric identity, $\cos 2\varphi = \cos^2\varphi - \sin^2\varphi$ in the above equation, the equation of the electrodes is determined,

$$r^2 \cos^2\varphi - r^2 \sin^2\varphi = k^2$$

This is of the form,

$$x^2 - y^2 = k^2$$

$$\left(\frac{x}{k}\right)^2 - \left(\frac{y}{k}\right)^2 = 1$$

This is the equation form of a hyperbola. So the ideal geometry dictates that each electrode of the quadrupole ion trap should be hyperbolic in cross section. Under these ideal conditions, the geometrical electrode surfaces follow the equipotential surfaces given by the solution. The potential has a known and constant value at every surface, as given by the applied voltage.

2.2 Description

A three-dimensional quadrupole ion trap with cylindrical symmetry is produced in a laminar approximation. The laminar constructed quadrupole ion trap consists of three electrodes, two end-cap electrodes and a body electrode. It is made up of several flat (laminar) steel plates having a hyperbolic cross section when stacked or arranged as layers one over the other. The ion trap constructed by the laminar plates is shown in Figure 2.1. The trap also has provision to mount the external electron impact ion source to it. The body electrodes are cut by a water knife (*Water Scythe, Inc*. in Beaumont, Texas) to approximate the hyperbolic electrodes. The figure 2.2 shows the schematic representation of the cross-section of the laminar constructed quadrupole ion trap.

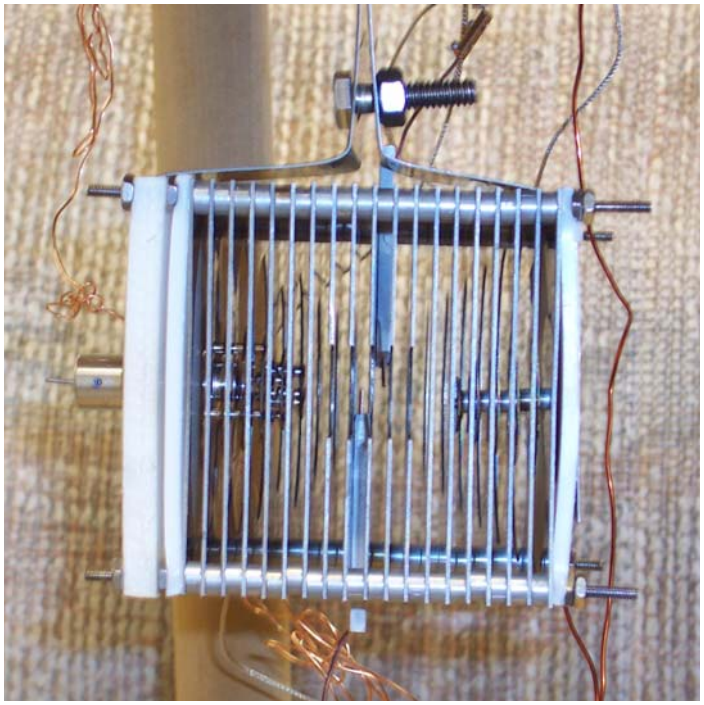

Figure 2.1 Picture of the laminar constructed quadrupole ion trap

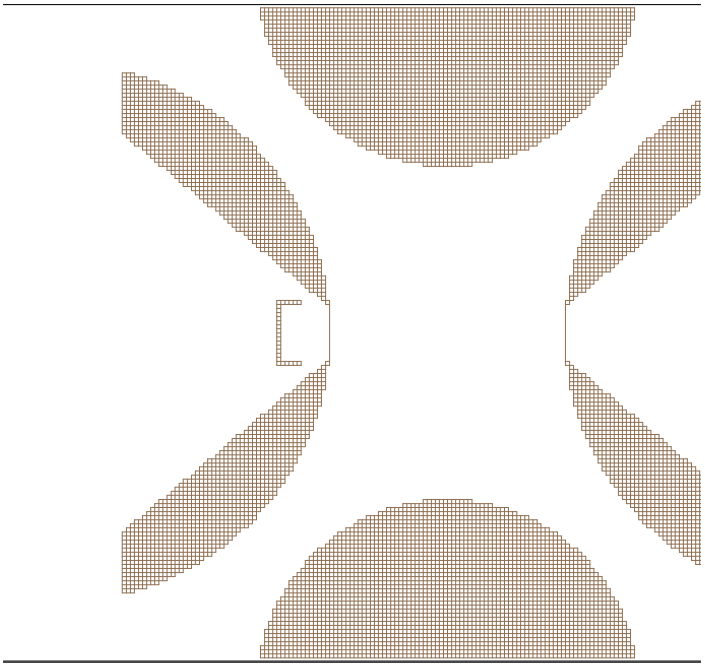

Figure2.2. Schematic diagram of the cross-section of the laminar constructed quadrupole ion trap

The electrodes are truncated for practical purposes, but in theory they extend to

infinity and meet the asymptotes. The asymptotes arise from the hyperboloid geometries of the electrodes [6]. The real advantage of the quadrupole is the lack of dependence of the ion secular oscillation frequency on the ion energy.

The laminar-approximated ion trap is easy to construct. Its electrodes can be cut with less difficulty. No numerically controlled lathes and mills are required. It can be made from hard to machine materials like tungsten or molybdenum. The internal field of the trap is very closely approximated to that of the ideal quadrupole by having electrodes that have hyperbolic cross-section. Figure 2.3 shows the comparison of the internal field (potential) in an ideal and a laminar constructed quadrupole ion trap. In the central part of the trap, the potential is nearly that of an ideal hyperbolic electrode but there are distortions at the edges due to the higher-order fields.

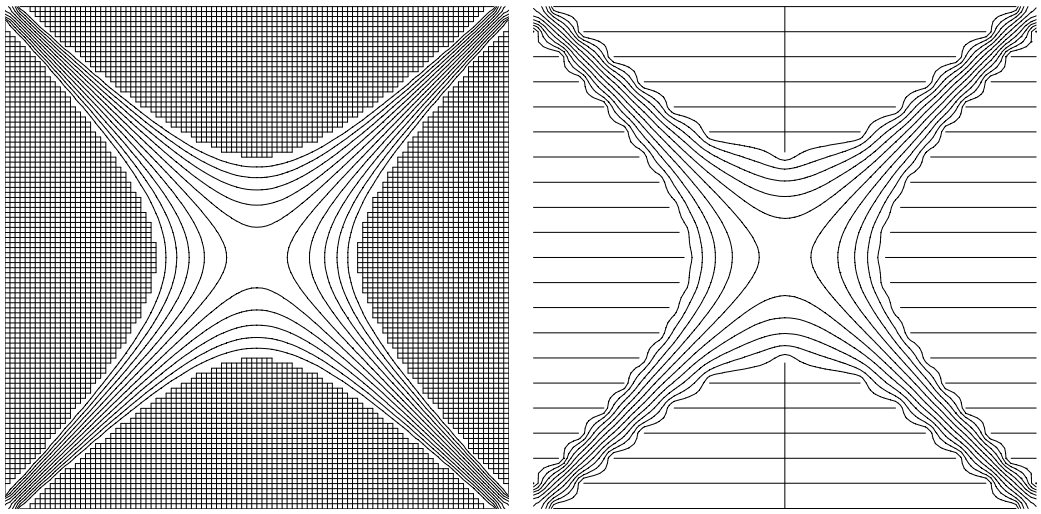

Figure 2.3 Comparison of the internal field in an ideal and the laminar construction quadrupole

The laminar construction provides more access into the trap through the interlaminar spaces without disruption of the field by the particle and optical

beams for reactions and spectroscopy to be performed. Due to the presence of several layers, there is better chance to tune the electric field inside the ion trap. The electrodes of the trap are non-solid, making it a lightweight instrument, which is more desirable as a field-portable unit.

Our instrument is run with opposite phases of RF on the end-cap electrodes and the body electrode. As a result, there is a conical nodal surface that has apex at the mid-point of the trap and extends between the two sets of electrodes. The laminar construction of the trap allows positioning the elements of interest at this nodal surface. Figure 2.4 shows the potential energy distribution inside the ion trap.

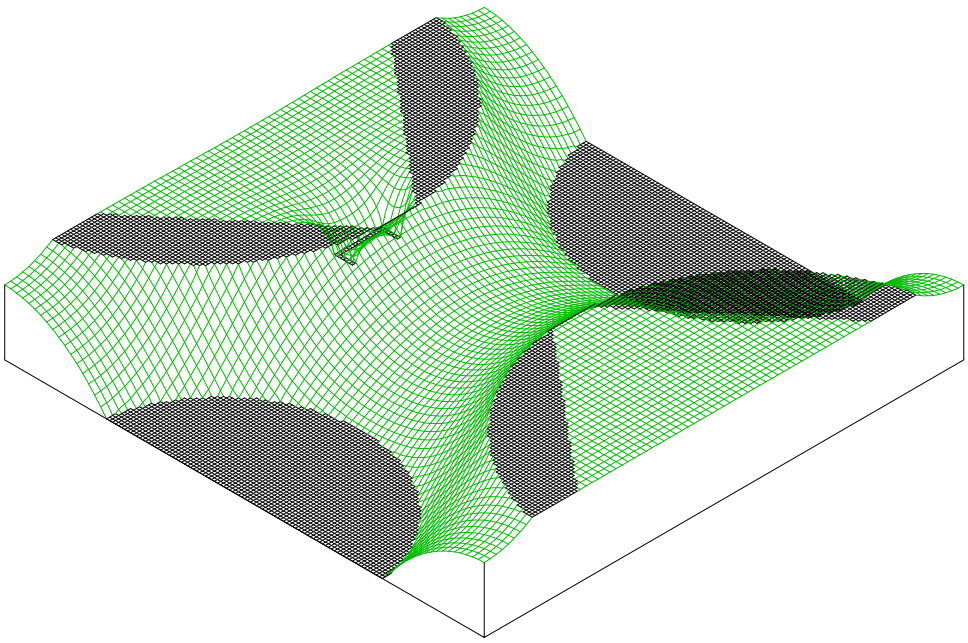

Figure 2.4 Potential energy distribution inside the trap generated by SIMION 3D

2.3 Theory

The theory behind the operation of the ion trap is best considered by examining the equations of the electric field within the trap of perfect quadrupolar geometry and of the resulting motion of ions in such a field [7]. The shape of the potential well developed within the ion trap when the electrodes are coupled to r.f. and d. c. potentials is described by

$$\phi_0 = \frac{1}{2}(U + V\cos\Omega t)\left(\frac{x^2 + y^2 - 2z^2}{r_0^2}\right) + \frac{U + V\cos\Omega t}{2}$$

where U and V are, respectively the maximum DC and RF potentials applied to the end-cap and ring electrodes, Ω is the angular frequency of oscillation of the RF potential and r_0 is the internal radius of the body electrode. This equation assumes that there is no appreciable space charge within the ion trap. The oscillation of the RF potential causes the field to periodically reverse in direction so that the ions are alternately focused and de-focused along the z axis, and vice versa in the radial plane.

The force acting on the motion of an ion [8] of mass m and charge ze, in such a field is derived from Newton's law:

$$F = -ze.\Delta\phi = m\vec{A}$$

from which the forces acting upon the ion in each of the perpendicular directions

are given by

$$\left(\frac{m}{e}\right)\ddot{x} + \left(U + V\cos\Omega t\right)\frac{x}{r_0^2} = 0$$

$$\left(\frac{m}{e}\right)\ddot{y} + \left(U + V\cos\Omega t\right)\frac{z}{r_0^2} = 0$$

$$\left(\frac{m}{e}\right)\ddot{z} - \left(U + V\cos\Omega t\right)\frac{z}{r_0^2} = 0$$

All the above expressions are homogeneous, linear, second order differential equations of the form:

$$\frac{d^2u}{d\xi^2} + \left(a_u + 2q_u\cos 2\xi\right)u = 0$$

which is known as the Mathieu equation [6, 7, 8] where a_u and q_u are dimensionless stability parameters for all the coordinates (u) in the x, y and z directions and ξ is also a dimensionless parameter equal to $\Omega t/2$ where Ω ($\Omega=2\pi f$) is the angular frequency of the RF drive potential applied to the body electrode and t is time. The a_u and q_u parameters are quite fundamental to the operation of the ion trap since they determine whether the ion motion is stable (i.e. the ions remain trapped) or unstable.

Solutions to the Mathieu equation are characterized as being either stable or unstable [8]. In stable solutions, u remains finite as ξ increases. In unstable solutions, u grows without bounds as ξ increases. From the well-known solutions to the Mathieu equation, a stability diagram is generated, characterizing the solutions to the derived equations of motion for an ion in the applied three-dimensional quadrupole field [5, 8]. Ions can be stored in the ion trap only if they are stable in both the r and z directions. Figure 2.5 shows the Mathieu stability diagram in (a_z, q_z) space for the QIT. It shows the common region in (a_z, q_z) space for which the radial and axial components of the ion trajectory are stable simultaneously. Any ion with a_z, q_z values outside the triangle are kicked off the trap. The coordinates of this stability diagram are the Mathieu parameters a_z and q_z which are defined as

$$a_z = -2a_x = -2a_y = -\frac{8eU}{mr_0^2\Omega^2}$$

$$q_z = -2q_x = -2q_y = -\frac{4eV}{mr_0^2\Omega^2}$$

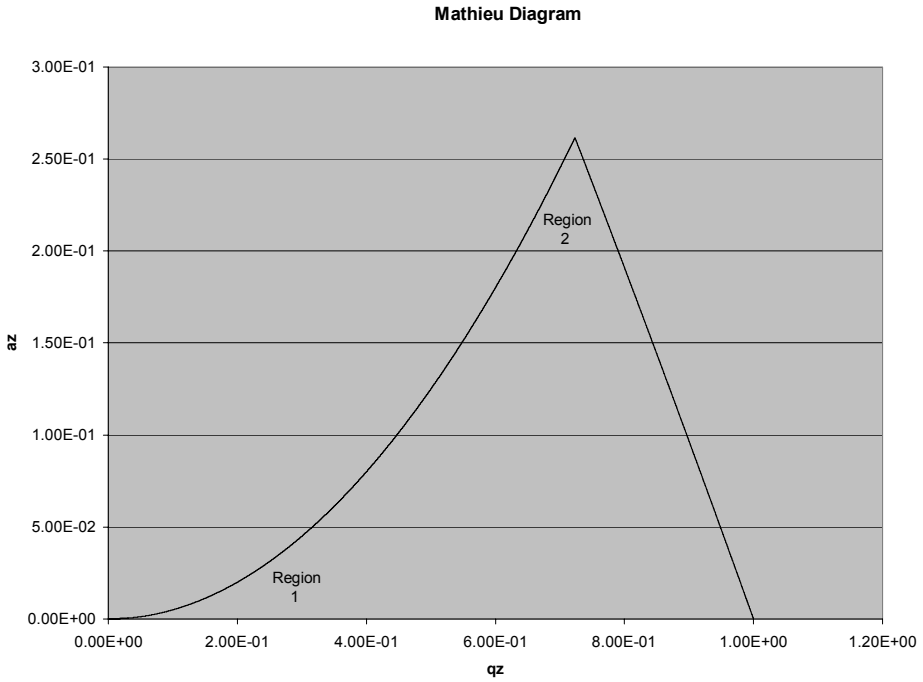

Figure 2.5 Lowest zone of stability of the Mathieu diagram in (a_z, q_z) space for the QIT

The triangularly shaped border lines of the above stability diagram are given by the equations:

$$a_z = \frac{1}{2} q_z^2$$

and

$$a_z = 1 - q_z - \frac{1}{8} q_z^2$$

The region at the top of the triangle i.e., Region 2 is the working zone of the mass-selective stability mode of operation, where the rf and dc are ramped together. Lines describing the detailed trajectories of the ions are drawn across the stability region. These are called as iso-β lines. The boundaries of the diagram correspond to β_r, $\beta_z = 0$ and β_r, $\beta_z = 1$. When an ion has a stable trajectory, its β_r

and β_z values must be between 0 and 1 and an ion developing an unstable trajectory is the one whose working point (a_z, q_z) has crossed one of these boundaries.

2.4 Ion Motion in Quadrupole fields

When the trapping parameters or the working point of an ion lies within the stability region, the ion is trapped successfully only when the bounds of its trajectory remain within the physical confines of the ion trap [9]. Under these conditions, the ion will assume a trajectory that resembles a figure-of-eight or Lissajous curve, which is defined by the radial and axial frequencies of ion motion.

The frequency with which an ion oscillates in the trap is called the secular frequency [5]. Figure 2.6 is a three-dimensional plot of an ion's trajectory in the laminar approximated quadrupole ion trap, generated by SIMION 3D [24]. The trajectory has the general appearance of a Lissajous curve, composed of two fundamental frequency components, $\omega_{r,0}$ and $\omega_{z,0}$ of the secular motion, with a superimposed micro motion of frequency $\Omega/2\pi$ Hz. The Lissajous trajectories of trapped ions are usually concentrated about the center of the ion trap. The frequency components are defined as

$$\omega_{r,0} = \frac{\beta_r \Omega}{2}$$

$$\omega_{z,0} = \frac{\beta_z \Omega}{2}$$

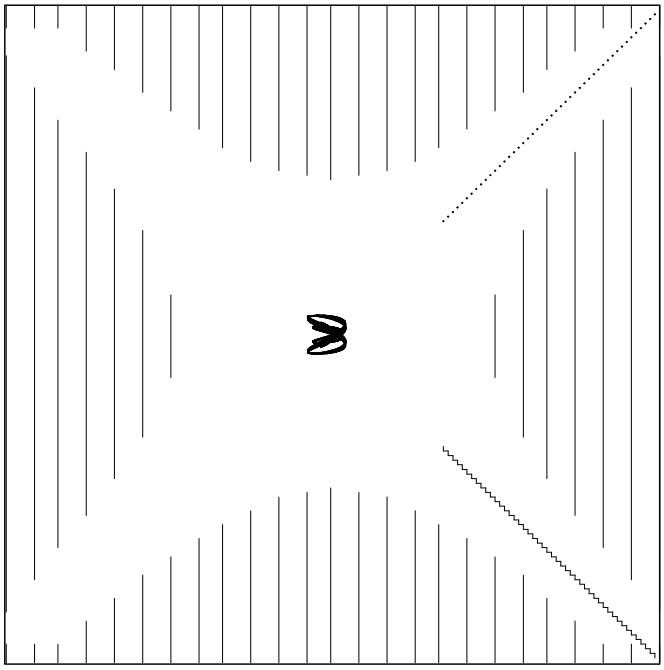

Figure 2.6. Three- dimensional representation of an ion's trajectory generated by SIMION 3D.

CHAPTER 3

EXPERIMENTAL SECTION

3.1 Vacuum system

The vacuum system of the analytical chamber includes a diffusion pump, mechanical pump, various valves (butterfly valve, fore line valve, roughing valve), and a thermostat. The diffusion pump is used to create vacuum by removing the molecules that make up the atmosphere inside the chamber. It cannot create vacuum with full atmospheric pressure inside the chamber. So a mechanical roughing pump (or fore pump) first brings the pressure inside the chamber down and then the vacuum diffusion pump takes over to create vacuum ranging from 10^{-3} to 10^{-10} Torr. The mechanical pump is also used to maintain proper discharge pressure conditions.

A vacuum diffusion pump is basically a stainless steel chamber containing vertically stacked cone shaped jet assemblies. A pool of specialized oil called Santovac 5 having a low vapor pressure is present at the base of the chamber. An electric heater present beneath the floor of the chamber heats this oil. The vaporized oil moves upward and is expelled through the jets. After exiting from the jet assemblies, the high-energy oil droplets collide and entrain the gas molecules that enter due to their thermal motion. This imparts a downward motion on the molecules in the space between the jet assemblies and the chamber

walls and transports them towards the pump outlet, creating higher vacuum. The oil molecules are condensed on the walls of the pump, which are cooled by the water that is circulated through coils on the outside of the chamber. Thus, a continuous cycle of vaporization, condensation and revaporization takes place. The base pressure created by the diffusion in inside our analytical chamber is in the range of 10^{-7} to 10^{-8} torr.

The mechanical pump (fore-line or backing pump) is rotary vane type, which physically sweeps the air from the system. The rotor is eccentric to the pump cavity. The rotating vane is kept in contact with the walls of the pump cavity by means of a compression spring. It is used to remove (rough) the bulk of the air from a system that is initially at atmospheric pressure and also to "back" the diffusion pump by removing the condensed molecules of gases. The fore line and fore line valve convey the discharge from the diffusion pump to the mechanical pump.

The polyphenyl ether (Santovac 5) fluid is used as the diffusion pump oil. It has high molecular weight, high thermal breakdown temperature, low vapor pressure, low reactivity, low toxicity, chemical inertness and heat of vaporization. This low vapor pressure oil captures air molecules, which are continuously removed by the fore pump to create usable vacuum. The oil is vaporized at a temperature range of 230-270ºC.

A special valve called the Butterfly valve is present between the diffusion pump and the analytical chamber. This valve is used to isolate the analytical chamber from the diffusion pump for the purpose of changing the filament and for

routine maintenance of the chamber.

3.2 Vacuum Control

The vacuum control is designed to turn the diffusion and mechanical pumps on and off and also to open and close the various valves. It includes a failure safety system consisting of a thermostat, alarm and time delay relay. These components insure that the diffusion pump is protected if the cooling system fails. The schematic diagram of the vacuum control system constructed is given in Figure 3.1.

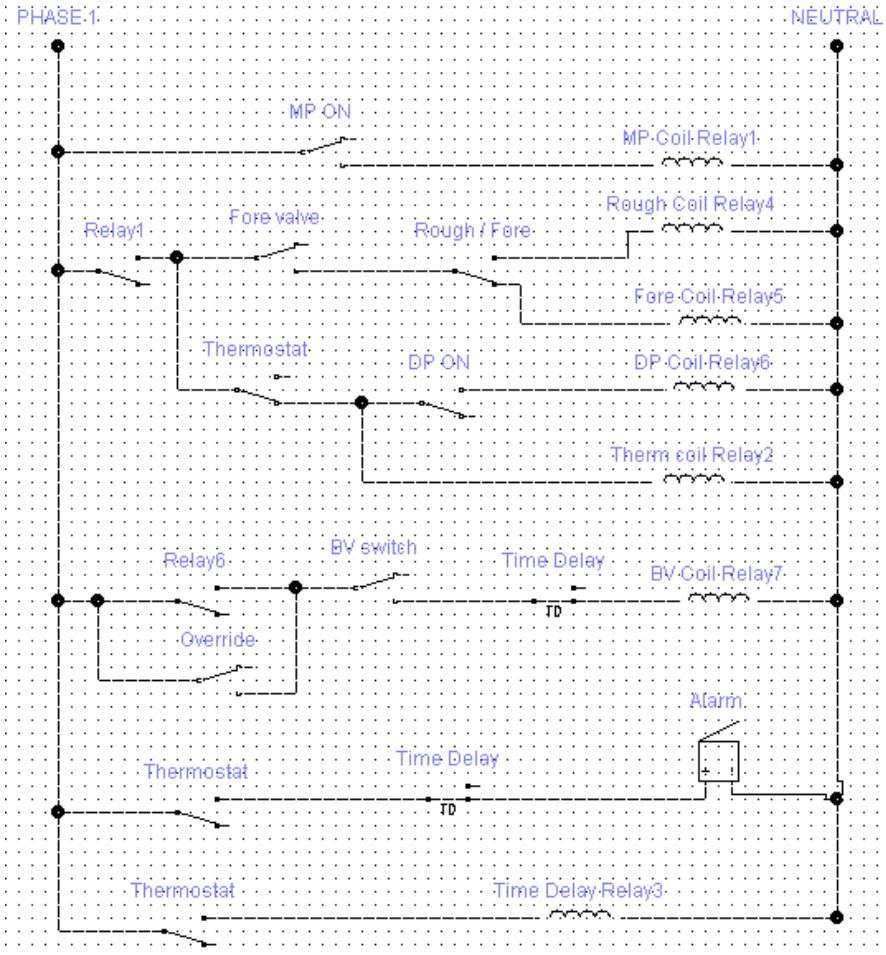

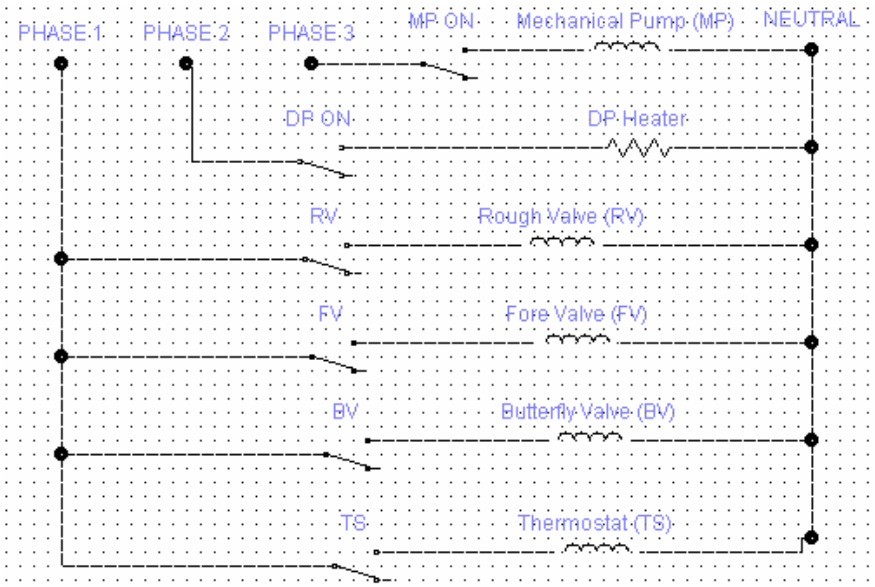

Figure 3.1 Basic layout of the Vacuum controller

3.3 RF generator

3.3.1 Description

A free running high voltage RF generator of the Utah type [10, 11] is constructed and used in all our experiments. It is a simple high voltage oscillator based around two 6146B vacuum tubes, which are cross-connected in a push-pull configuration. The output is the voltage across the oscillator tank circuit. The tank circuit consists of an adjustable tapped coil and a high voltage variable capacitor in parallel, which determines the frequency of the generator. The coil can be tapped at various positions to vary the inductance for coarse frequency adjustments. The taps are made with small alligator clips, which can be adjusted to balance the RF and set the frequency range the capacitor can tune. Leaving one side fixed, and slightly adjusting the other side balances the RF. Moving the taps in towards the center increases the frequency and moving them out decreases the

frequency. The taps are placed symmetrical about the center of the coil. The variable capacitor in parallel with the load is used for fine frequency adjustments.

An external high voltage DC supply is used to power the oscillator circuit. It is variable from 0V to 300V and connected to the generator through the side panel MHV connector. The RF voltage delivered to the load (ion trap) is totally determined by the high voltage DC supply voltage. There are two output connections of the RF signal that are 180° out of phase. The output is a differential output. The two outputs phases from the RF generator are each coupled directly to the load through large value capacitors (one fixed and one variable). A built in low voltage supply is coupled to the RF output to give a low DC differential voltage between the two RF output phases.

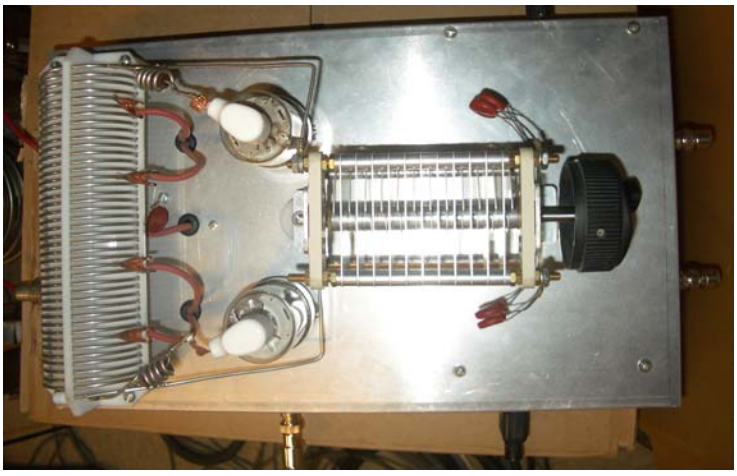

Figure 3.2 Top view of the RF generator

Major components of the RF generator can be seen in the above picture. The generator is constructed on a small aluminum chassis with the main tuning capacitor, tank coil and two vacuum tubes on the top and other components in the

bottom. The tank coil is hand wound on two plastic plates. In order to minimize the stray capacity all the RF components are placed in such a way that the leads are as short as possible. The tubes are mounted symmetrically close to the coil. The connections for the high voltage DC supply and the DC float supply are seen along the side. The coil and capacitor are insulated from the chassis by plastic mounting hardware.

3.3.2 Basic Operation

The generator is plugged into a standard AC outlet. The AC powers a transformer that in turn powers the filaments in the two oscillator tubes. The high voltage comes from the external DC power supply. The float DC is from another external power supply. This float DC voltage is applied on both the output phases. When no external DC float voltage is used, the float input connector on the side panel of the generator is grounded. RF balance is attained on the two output phases by adjusting the tap positions on the internal coil. The capacitors (fixed and variable) set the frequency of the RF generator to the appropriate operating frequency. When the capacitive reactance equals the inductive reactance, the LC circuit (where L is the inductance and C is the capacitance) oscillates stably. The resonant frequency is given by the equation

$$F_r = \frac{1}{2\pi\sqrt{LC}}$$

The RF generator constructed is not crystal-stabilized and so exhibits a frequency variation of ~1%. It is always operated in the continuous mode in our experiments.

3.4 Detector

Channel Electron Multiplier (channeltron) [12] is used as the detector in the quadrupole ion trap. A channeltron is a horn-shaped continuous dynode structure that is coated on the inside with an electron emissive material.

The basic physical process that allows an electron multiplier to operate is called secondary electron emission. When an ion strikes the channeltron on the input surface, secondary electrons are created that produce an avalanche effect to create more secondary electrons and finally a current pulse. Alkali dopents within the emissive layer lower the work function of the surface leading to increased secondary emission. As the secondary electrons travel down the channel, they repeatedly collide with the channel wall, producing still more secondary electrons as shown in the figure 3.3. The electrons are accelerated towards the anode end of the channel by the ever-increasing positive potential within the channel produced by the resistive lead glass layer beneath the emissive layer. This process is repeated until the resulting cloud of electrons exits the channel and is collected by the anode. Varying the voltage across the channeltron alters both the electron trajectory and the number of secondary electrons produced per strike. So by altering the voltage across the channeltron, the gain of the device is varied.

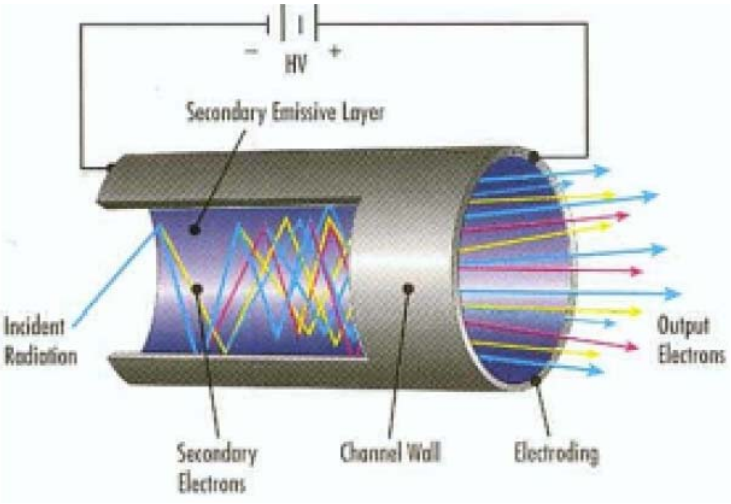

Figure 3.3 The multiplication process in a Channel Electron Multiplier

In all our experiments the channeltron is used in the analog mode. It is operated at a minimum voltage of 1500V. The multiplier is preconditioned with the input signal to degas the device.

3.5 Ion source

An electron impact (EI) source is mounted external to the trap. The body electrode has a center hole to allow the ion source to be mounted. Ions are created in the trapping region with an electron beam. The electron beam is produced from a filament formed by a coil of thoriated tungsten wire of 10mm width. On passing current through the tungsten wire, it gets heated and produces an electron beam. An electron from the beam knocks an electron off of analyte (air) atoms to create ions on collision. Figure 3.4 shows the ion source mounted externally to the ion trap in our lab.

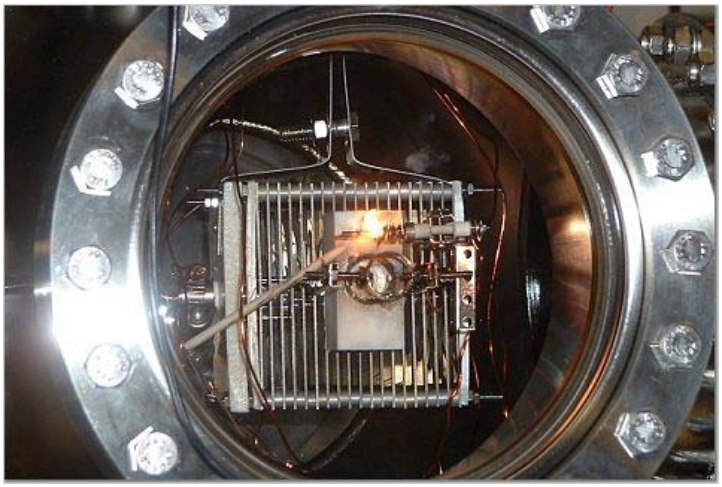

Figure 3.4 Picture of the Quadrupole Ion trap instrument working in our lab

The filament is biased at a voltage of -50 to -100 V. A lens system that stops just before the ring electrode is used to accelerate electrons to pass into the trapping region. A voltage of 100V is applied to the lens while the grid of the filament is grounded. Typically, 2-2.25 A of current is passed through the electron filament during loading.

CHAPTER 4

RESULTS AND DISCUSSIONS

Mass spectra of the background gases present in the analytical chamber are obtained in two different operational modes of the laminar constructed quadrupole ion trap. Mass selective instability and Mass selective trapping modes are employed. All the data used the RF drive frequency of 1.3MHz.

4.1 Mass-selective Instability

This technique involves the external detection of mass-selective self-ejected ions whose trajectories have become unstable [4]. Ions are created within the trap by injection of electrons and a range of m/z values are held in bound or so-called stable orbits by virtue of the RF potential. As the amplitude of the RF potential is increased, the motion of the ions becomes progressively more energetic, such that eventually they develop unbound (unstable) trajectories along the axis of symmetry (the z-axis). Then in order of increasing m/z values the ions exit the device and impinge on a detector.

The electrodes are driven at an initial RF voltage V_0 and a fixed frequency such that all ions in the m/z range of interest are trapped within the imposed quadrupole field. No DC voltage is applied (U=0) between the electrodes, making the field purely oscillatory. This means that the locus of all possible values of m/z

maps directly onto the q_z axis on the stability diagram. The RF amplitude is then ramped linearly so that the a_z, q_z values of the ions are moved in the $\beta_z = 1$ boundary where upon the ions are ejected in increasing order of the m/z value. The trapping conditions within the quadrupole field are manipulated so that ions of a selected mass are caused to have unstable trajectories by virtue of the fact that their amplitude of oscillation in the axial direction increases very sharply at the boundary point on the stability diagram ($q_z = 0.91$, $a_z = 0$) [1].

Graphs 4.1 and 4.2 show the mass spectrum of the background gases present in the chamber. Graph 4.2 is the differentiated form of the Graph 4.1. The bottom axis is also changed from RF amplitude to m/z units.

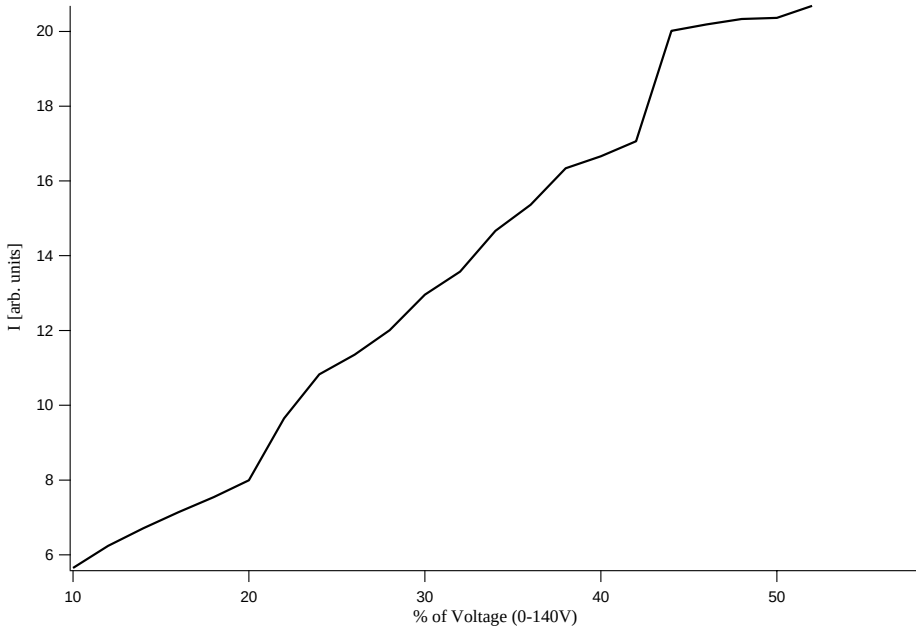

Graph 4.1 Integral form of the mass spectrum in Mass-selective instability mode

The spectrum shows the basic components of air. The peaks are very broad and

the resolution is about 7, indicating low resolution of the instrument. There are many factors that are limiting the resolution. The instrument is run in cw mode, which may cause space-charge effects due to large number of ions inside the trap. Trap loading or saturation of the trap is well shown in Graph 4.3.

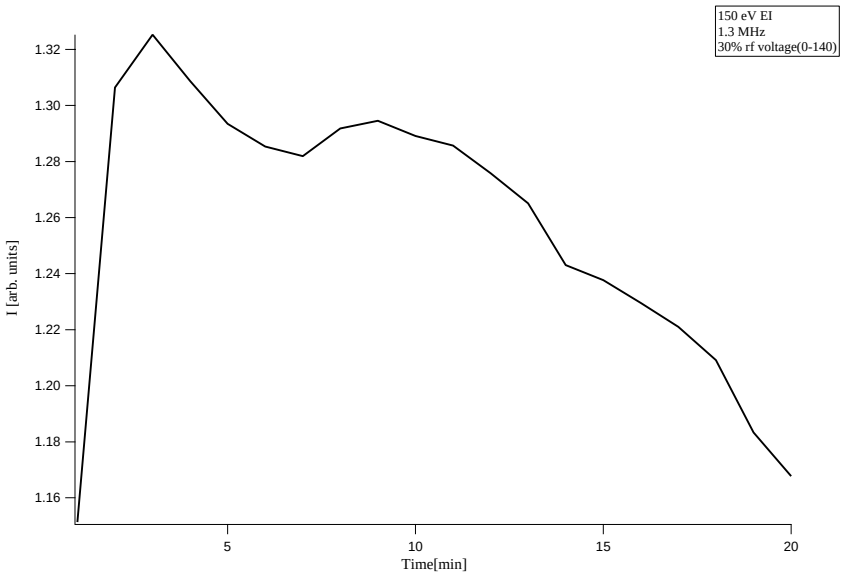

Graph 4.3 Saturation curve

4.2 Mass-selective trapping mode

The mass-selective trapping mode of operation involves trapping of ions according to their m/z ratios and then detecting them by pulse ejecting from the trap into an external detector [1]. It involves selecting a working region of the stability diagram where only ions with a single value of m/z possess stable trajectories and hence are stored. To generate a mass spectrum the amplitudes of the DC and RF fields are scanned slowly. An example of the recording of peaks in the mass spectrum of background gases is shown in Graph 4.4.

The mass spectrum is obtained by operating the instrument in cw, mass-selective trapping mode. Ions are injected continuously into the trap through the lens and both the RF and DC voltages are ramped. As the voltages are ramped, only one mass at a time is stable in the trap. All the rest are ejected, so that the presence of a mass is indicated by a decrease in the ion current detected at the channeltron.

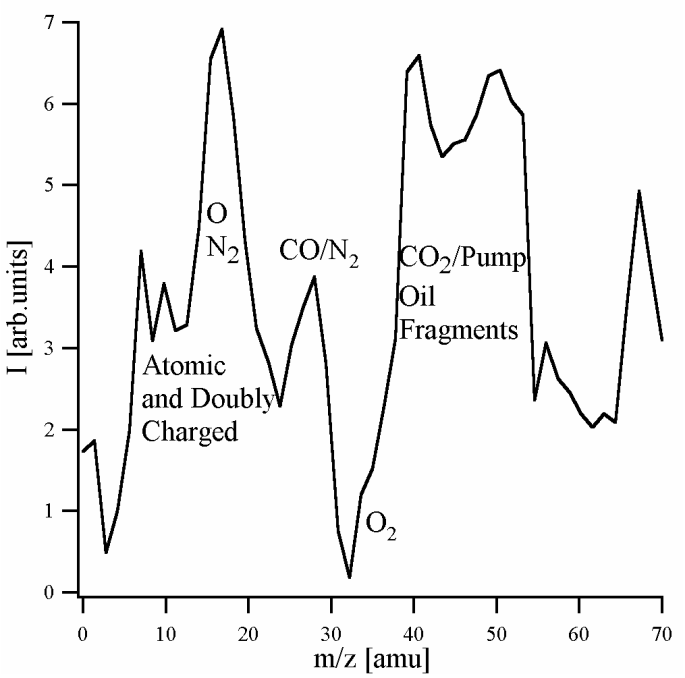

Graph 4.4 Mass spectrum of the background gases by Mass-selective trapping mode

The channeltron is used in the analog mode, reading the output current as the signal. Large currents are used to get reliable signal. These large number of ions in the trap resulted in the loss of resolution as the space-charge repulsion of the ion cloud disturbs the internal potential field. The space-charge effect broadens the ion energy distribution and reduces the mass resolution. Figure 4.5 shows the loading of the trap for different time intervals. It is done by monitoring

ions' current vs time (time-dependent studies). At low RF, the space charge is built on longer intervals of time.

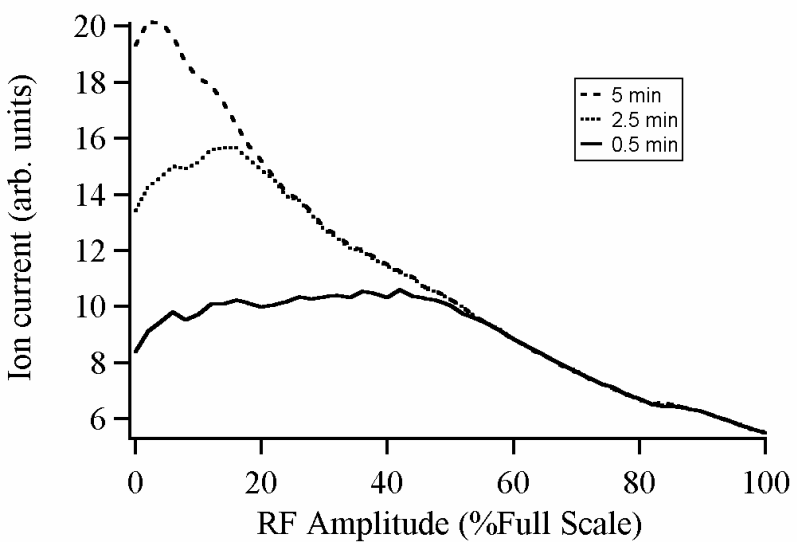

Graph 4.5 Trap loading

CHAPTER 5

FOURIER DETECTION

5.1 Introduction

The Fourier transform is a generalization of the Fourier series. Fourier series uses a discrete set of frequencies which are summed over. The Fourier transform integrates over a continuous set of frequencies. For a signal or function f (t), the Fourier transform is defined as

$$F(\omega) = \int_{-\infty}^{\infty} f(t) e^{-i\omega t} dt$$

and the inverse Fourier transform is defined as

$$f(t) = \frac{1}{2\pi} \int_{-\infty}^{\infty} F(\omega) e^{i\omega t} d\omega$$

where i is the imaginary number, defined as $\sqrt{-1}$ and $\omega = 2\pi f$, is the range of angular frequencies associated with the signal. The Fourier Transform is used to

analyze the frequency content of the signal. The analyte can be studied non-destructively by the Fourier detection. It converts functions from time domain to the frequency domain. The Fourier transform mode is not energy limited.

A discrete Fourier transform is the Fourier transform of the discrete values defined as

$$F(k\Delta f) = \sum_{n=0}^{N-1} f(n\Delta t) e^{-i(2\pi\ k\Delta f)(n\Delta t)} \qquad \text{for k = 0, 1, 2, ..., N-1}$$

The fast Fourier transform (FFT) is a discrete Fourier transform that is faster to calculate on a computer. The Nyquist criterion states that for a sampling frequency, fs, reliable frequency information can be obtained for only frequencies less than fs/2. For most of the FFTs, the computer algorithm restricts N to a power of 2 such as 64, 128, 256 and so on. Only the magnitude or the amplitude of the complex number generated by the FFT is actually used. A plot of the magnitude of the FFT output, as a function of frequency is called the power spectrum or the frequency spectrum.

The signal starts and ends at different phases in the cycle, leading to leakage of the signal. A process called windowing can reduce this. The fundamental concept of windowing is that if the amplitude of the signal at both ends (near t=0 and near t=T) is reduced to zero in a smooth fashion, the end effects will not be serious. The windowing operation emphasizes the middle portion of the time trace, and de-emphasizes the ends. The signal is multiplied by a windowing function, which starts at zero at t=0, increases smoothly to 1 at

t=T/2, and then decrease smoothly again to zero at t=T. The most common windowing function is the Hanning window, created by a simple cosine wave. The Hanning window function u (t) is defined as

$$u(t) = \frac{1}{2}\left[1 - \cos\left(\frac{2\pi t}{T}\right)\right] \quad for \;\; 0 \le t \le T$$

The Hanning window operation causes a loss of information near the end points of the signal. This leads to an overall reduction in the amplitude of the frequency spectrum. To compensate this, the amplitude of the FFT is multiplied by a factor of $\sqrt{8/3}$. Windowing reduces but does not totally eliminate the leakage of the signal.

5.2 Experimental section

5.2.1 Description

The experimental setup for the Fourier transform nondestructive detection uses a small pin electrode, embedded in homemade ceramic piece to provide electrical insulation. Two pin electrodes are placed in the potential well region of the trap through the interlaminar spaces. They are placed symmetrically opposite to each other in between the two end-cap electrodes and can slide in and out to optimize the position. They detect the current induced by the oscillating ions in the trap. The induced current is periodic in nature and is related to the mass/charge ratio of the ions. The pin position has a significant effect on the measured frequency of the trapped ions. It reduces the pickup of the RF trapping voltage, which would otherwise saturate the preamplifier. RF voltage is applied to both the end-cap and

body electrodes for sometime to trap the ions inside the potential well. These trapped ions oscillate in the z-direction at their characteristic secular frequencies. The secular frequency in the z-direction is dependent upon the m/z ratio of the ions, at a fixed RF trapping voltage and frequency.

5.2.2 Operation

Image currents induced on the pin electrodes are converted to voltages and amplified with a homemade differential amplifier circuit. After amplification, the output voltage is filtered with a low-pass filter set at a frequency break point of 2MHz. The image current signal is recorded using a Le Croy LC574AL fast digital oscilloscope [13] and Fourier transformed to obtain intensity vs. frequency spectrum. An in-house program is used to manage the scope-to-PC interface. Data is obtained at fixed conditions of RF voltage and amplitude. The pin electrodes detect every stable ion at one time. The oscilloscope collects the data points and sends them to the computer. The program in the computer averages the data and employs a fast Fourier transform algorithm to calculate the frequency spectrum from the averaged time domain data. Simple calibration procedures are used to convert this spectrum to a mass spectrum. The Figure 4.1 shows the block diagram of the of the Fourier detection of the ion's signal in our lab. The oscilloscope is operated at a time interval of 5μsec and a voltage of 100mV.

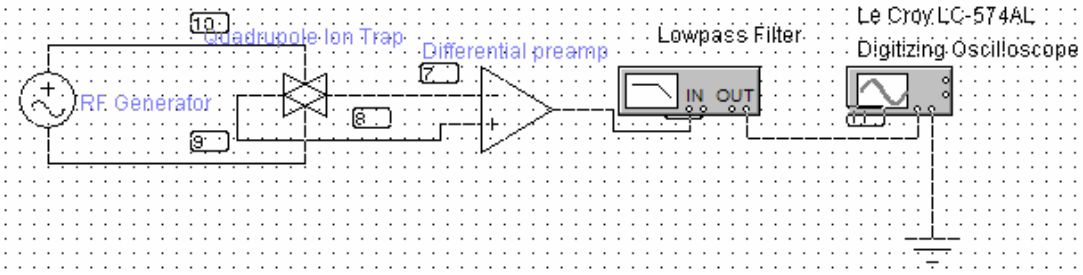

Figure 5.1 Block diagram of the Fourier detection

To avoid aliasing errors entirely, the signal is filtered before calculating the FFT. A low-pass filter is used to eliminate aliasing, and is called an anti-aliasing filter. A low-pass filter lets low frequency components of the signal to pass through, but cuts off frequency components above some cut-off frequency. Ideally, the cut-off frequency should be one-half of the sampling frequency to avoid aliasing (Nyquist criterion). The low-pass filter is discussed in detail in 5.2.3

5.2.3 Low Pass Filter

A low-pass filter is a device that allows all signals below a certain cutoff frequency to pass while attenuating all others. The circuit is essentially a frequency-sensitive voltage divider. At high frequencies the output behaves as if it is shorted while at low frequencies the output appears as an open circuit. The attenuation slope of the filter is dependent upon the order of the network which is equal to the number of reactive elements in the low-pass filter.

At some frequency, the inductor and capacitor will become resonant and peak the response if the load is high enough. The resonant frequency can be determined by

$$F_r = \frac{1}{2\pi\sqrt{LC}}$$

where L and C are the inductance and capacitance of the respective components of the filter.

A Butterworth filter is a medium-Q filter whose response is the flattest pass band response available and contains no ripple. The attenuation of a Butterworth filter is given by

$$A = 10\log_{10}\left[1+\left(\frac{f}{f_c}\right)^{2k}\right]$$

where, f is the frequency at which attenuation is desired, f_c is the cut-off frequency (at 3.01dB) of the filter and k is the number of circuit elements.

A 5-element Butterworth low-pass filter is built and used in filtering the data used for the Fourier transform. Firstly the order of the filter (number of elements, k) is determined by the attenuation curve and then the corresponding network configuration is found. The elemental values of the normalized 5-element low-pass filter for a cut-off frequency of one radian per second (0.159 Hz) and a load resistance of one ohm are determined from the filter tables. Each normalized element value is then scaled to the cut-off frequency of 2MHz and load resistance of 50ohms using the formulae given below

$$L = \frac{R}{2\pi f_c} L_{prototype} \qquad ; \qquad C = \frac{1}{2\pi f_c R} C_{prototype}$$

The schematic diagram of the constructed filter is shown in the Figure 5.2. The 5-element Butterworth filter provides an attenuation of approximately 30dB at a frequency equal to twice the cutoff frequency of the filter.

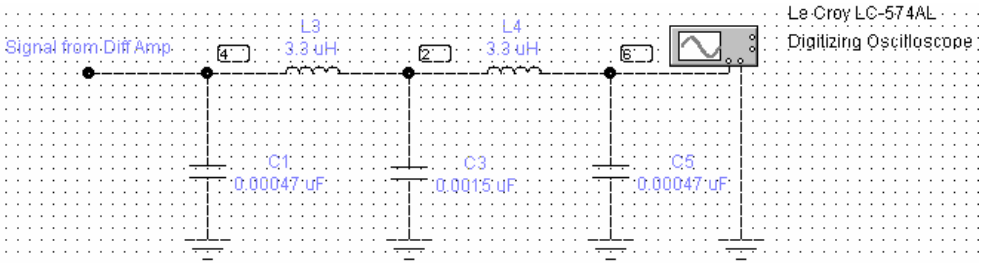

Figure 5.2 Schematic representation of the Butterworth Low-pass filter

5.2.4 Pulsing circuit

A pulsing circuit with two 8-pin 555 timers is used to produce a pulse of time period of 5μsecond for Fourier detection. It used a supply voltage of +15V. The first 555 timer is connected in the astable mode, producing a square wave. The circuit is called an astable because it is not stable in any one state and the output is continuously changing between the low (0V) and high (+15V). The frequency of the operation of the astable circuit is dependent upon the values of R1, R2 and C1 and is calculated by the formula:

$$f = \frac{1.44}{(R_1 + 2R_2)C_1}$$

where f is the frequency in hertz, R1 and R2 are in ohms and C is in farads. The components of the circuit are determined using the above formula with frequency of 100Hz.

The second 555 timer is operated in the monostable mode which produces a single output pulse when triggered. The duration of the pulse is called the time period (T) and is given by the resistor R and capacitor C as:

$$t = 1.1RC$$

where R is in ohms and C is in farads. The schematic diagram of the pulsing circuit used is given in Figure 5.3. It shows the actual values of the resistors and capacitors used to produce a single output pulse of 5μsec duration. The capacitor between the output of the first 555 and the trigger input of the second differentiates the pulse, so only a single trigger event is received.

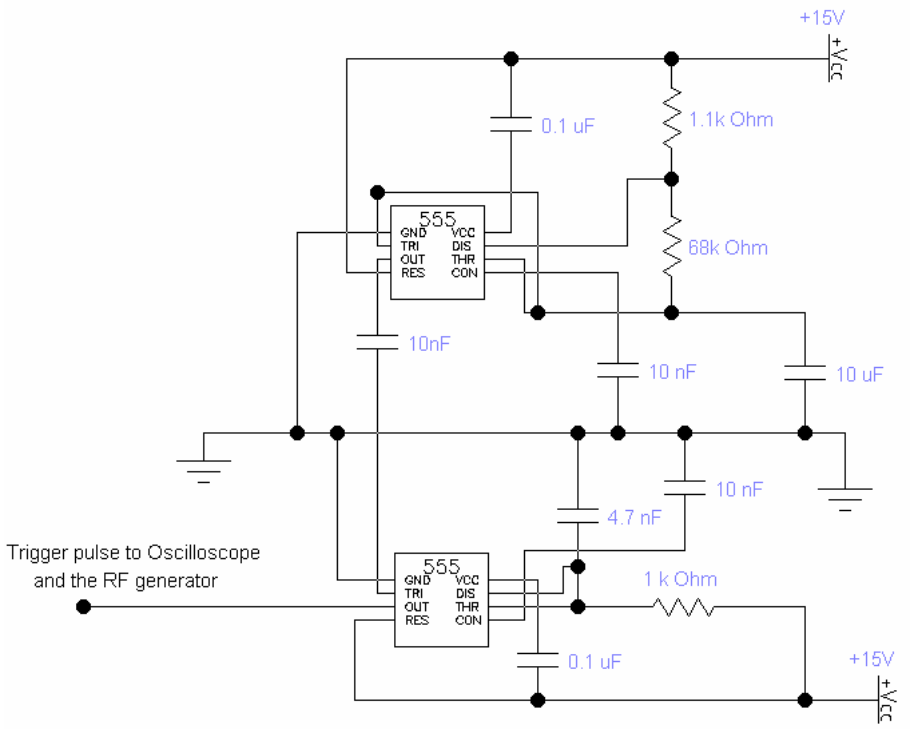

Figure 5.3 Schematic representation of the pulsing generator

5.2.4 Differential Amplifier

The differential amplifier amplifies the difference between two input signals (-) and (+). It is also called a differential-input single-ended output amplifier. It is a precision voltage difference amplifier. This amplifier uses both inverting and non-inverting inputs with a gain of one to produce an output equal to the difference between the inputs. Two buffer amplifiers are also used to remove the limitation of its performance by the low input impedance.

A surface mount differential amplifier circuit is constructed using OPA129 to amplify the ion's signal, shown in Figure 5.5. It amplifies the difference between the two output voltages of the signal and rejects the noise common to both the output voltages due to RF pick up. The gain of the differential amplifier is changed by adjusting the variable resistors and capacitors.

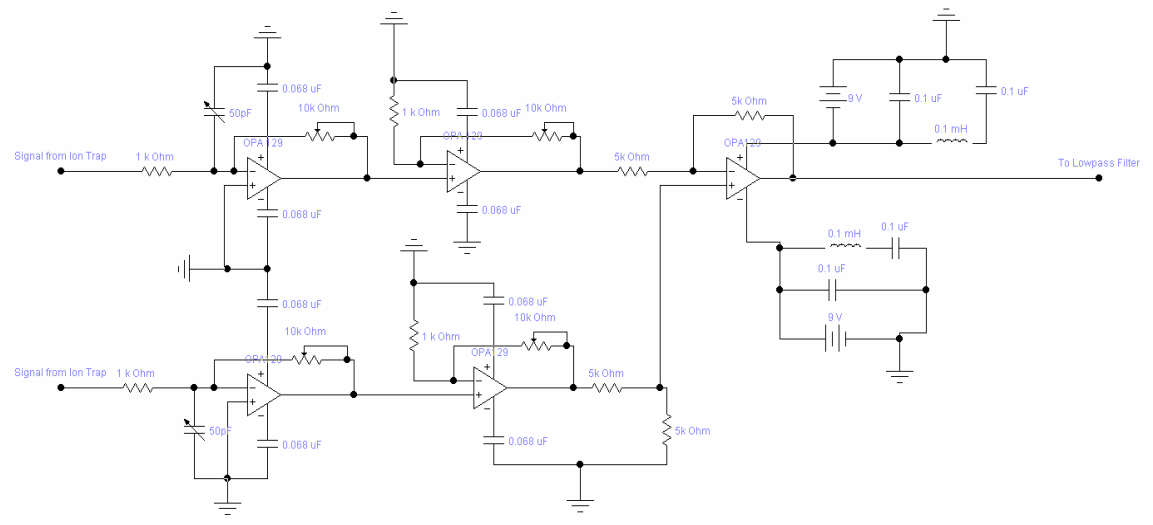

Figure 5.4 Schematic diagram of the constructed differential amplifier

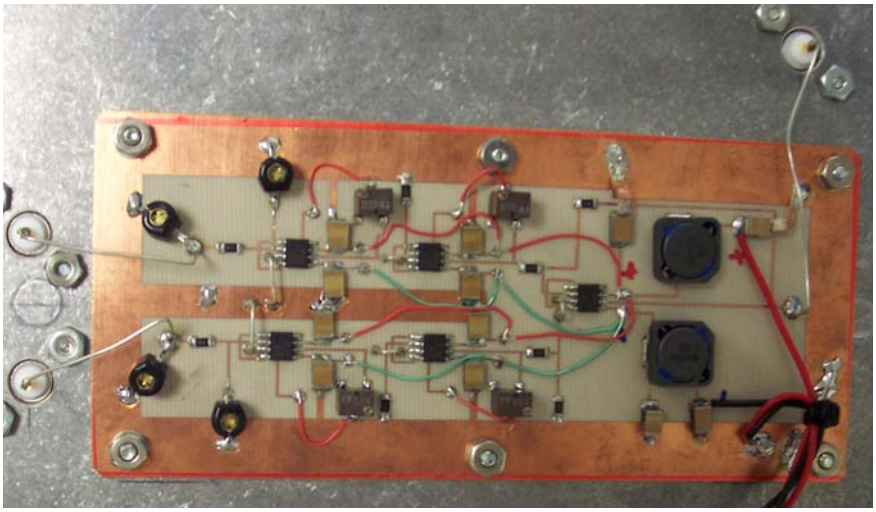

Figure 5.5 Picture of the constructed differential amplifier

5.3 Results and Discussion

Graph 5.1 shows the power spectrum of the background gases by Fourier transforming the data obtained by loading the trap for 5min at a RF voltage of 200V, RF frequency of 1.6MHz and filament current of 2.25amp. The m/z ratio is plotted along the x-axis and intensity of the signal is plotted along the y-axis. In spite of the high background, four dominant peaks are seen at 12, 14, 20, 29.5 of m/z. Background noise is due to the spikes, produced by the loss of data points during the transfer from the scope to the computer. Noise is also due to the RF pick from the generator. Due to the presence of large background noise and broadening of the signal, the resolution of the instrument could not be found.

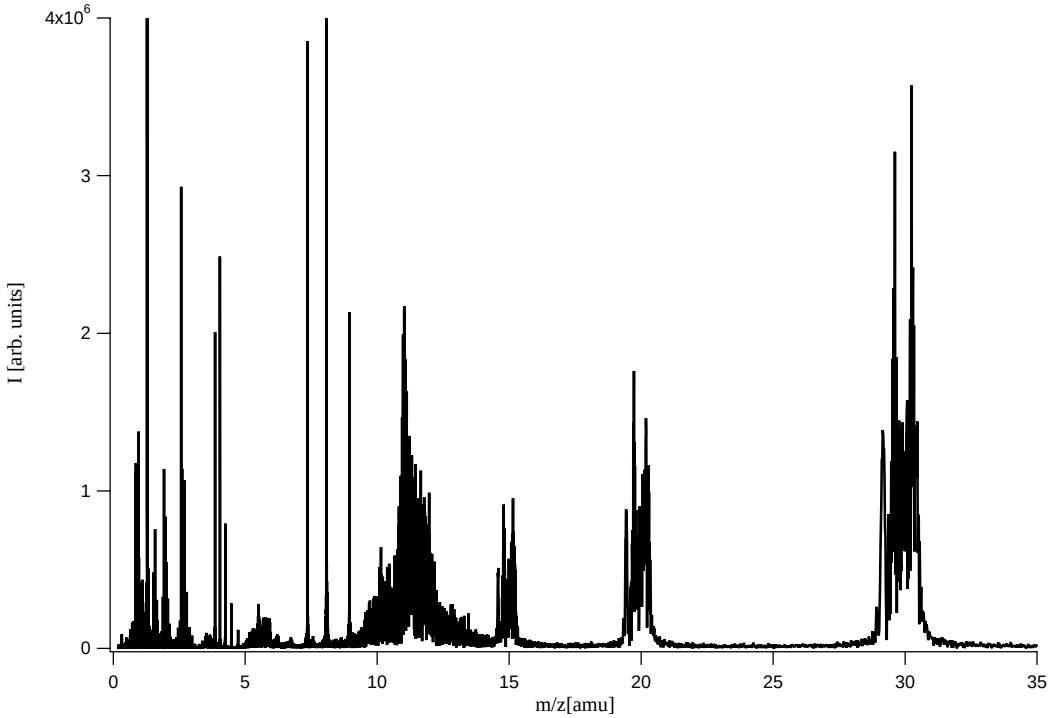

Graph 5.1 Power spectrum of the background gases

CHAPTER 6

CONCLUSIONS & FUTURE DIRECTIONS

6.1 Conclusions

Hyperbolic geometry is well approximated in the laminar constructed quadrupole ion trap. A quadrupole ion trap with laminar approximation has been constructed. The laminar approximation of the electrodes has many advantages. There is more access for particle and photon probes through interlaminar spaces to facilitate in-trap dissociation experiments. These traps are versatile and easy to construct. A higher mass range can be obtained by lowering the operating frequency. It can also be approximated to higher-order multipoles.

Resolution of our instrument is limited by the external hardware. There is not good enough data quality and so not a good enough spectrum to predict its resolution. A few changes to the instrumentation of the trap will help in obtaining good quality data, which will improve the resolution.

6.2 Future directions

The resolution of the instrument (in non-FT studies) is energy limited. We are not cooling the ions. This may cause broadening of the ions signal. So by using a buffer gas [He] to dampen the ions can result in better resolution.

Improvements in injection, RF electronics and detection will allow improvement of the resolution of the instrument. The channeltron is used in the analog mode, reading the output current as the signal. In order to get reliable signals, relatively large ion currents must be used. These large ion currents result in a large degree of space-charge repulsion in the trap, which broadens the ion energy distribution and reduces the mass resolution. Improvements in detection system will allow us to work at lower ionic currents, which should improve resolution. The dynamic range of the instrument can be improved by compensating the space-charge effects. Switching to pulse-counting mode will improve resolution. Changing the body electrode to minimize the space-charge effects will allow working at higher order fields with better resolution.

The RF generator used shows a frequency variation of ~1%. Since the stability parameters depend on the square of the frequency, there is a 2% limit for resolution. Minimizing the RF pick by the trap will also reduce the noise. This can be done by placing the RF generator in a closed, electrically isolated box.

The current injection/extraction lens system is inadequate. It does not extend through the body electrode, rather it stops just before and ions must fly through the interlaminar space. Construction of injection lens, which extends to the edge of the body electrode and opens in the interior of the trap, will overcome the inadequate injection of ions.

LIST OF REFERENCES

[1] March, R. E.; Hughes, R. J. *Quadrupole Storage Mass Spectrometry*; Wiley-Interscience: New York, 1989.

[2] Nourse, B. D.; Cooks, R. G. *Anal. Chimica Acta*, **1990,** 228, 1-21

[3] Paul W. *Rev. Mod. Phys*. **1990,** 62, 531–540.

[4] March, R. E.; Todd, J. F. J. (Eds) *Practical Aspects of Ion Trap Mass Spectrometry*, Vols 1, 2 and 3; CRC Press: Boca Raton, FL, 1995.

[5] Gerlish, D. *Advances in Chemical Physics,* "Inhomogeneous rf fields: A versatile tool for the study of processes with slow ions", **1992**, 82, 1-176.

[6] March, R. E. *J. Mass Spectrom.* **1997,** 32, 351- 369.

[7] Todd, J. F. J.; Penman, A. D. *Intl. J. Mass Spectrom. Ion Processes* **1991,** 106, 1-20.

[8] Stafford, G. C.; Kelley, P. E.; Syka, J. E. P.; Reynolds, W. E.; Todd, J. F. J. *Intl. J. Mass Spectrom. Ion Processes* **1984,** 60, 85-98.

[9] Forbes, M.W.; Sharifi, M.; Croley, T.; Lausevic, Z.; March, R.E. *J. Mass Spectrom.* **1999,** 34, 1219- 1239.

[10] Jones, R. M.; Gerlish, D.; Anderson, S. L. Rev. Sci. Instrum. 1997, 68 (9), 3357-3362.

[11] Jones, R. M.; Anderson, S. L. Rev. Sci. Instrum. 2000, 71 (11), 4335-4337.

[12] Model 7800, De Tech Inc.

[13] LC574AL fast digital oscilloscope, Lecroy

[14] Badman, E. R.; Cooks, R. G. *Anal. Chem*. **2000,** 72, 5079-5086.

[15] March, R. E. *Intl. J. Mass Spectrom. Ion Processes* **1992,** 118/119, 71- 135.

[16] Badman, E. R.; Cooks, R. G. *J. Mass Spectrom*. **2000,** 35, 659-671.

[17] Badman, E. R.; Johnson, R. C.; Plass, W. R.; Cooks, R. G. *Anal. Chem*. **1998,** 70, 4986-4901.

[18] Badman, E. R.; Wells, J. M.; Bui, H. A.; Cooks, R. G. *Anal. Chem*. **1998,** 70, 3545-3547.

[19] Todd, J. F. J.; March, R. E. *Intl. J. Mass Spectrom*. **1999,** 190/191, 9-35.

[20] Amster, I. J. *J. Mass Spectrom.* **1996,** 31 (12), 1325-1337.

[21] Hars, G.; Maros, I. *Intl. J. Mass Spectrom.* **2003,** 225, 101-114.

[22] March, R. E. *Intl. J. Mass Spectrom. Ion Processes* **1992,** 118/119, 71-135.

[23] March, R. E. *Rapid Commun. Mass Spectrom.* **1998,** 12, 1543-1554.

[24] SIMION 3D by David Dahl at Idaho National Engineering Labs, USA.

APPENDIX

VITA

Nagalakshmi Tentu was born on September 7th, 1979, in Hyderabad, India. She received her Bachelors Degree in Pharmacy from Osmania University, India, in September 2002. In the Spring of 2003, she came to the University of New Orleans, New Orleans, Louisiana to pursue her Masters degree in Chemistry under the supervision of Dr. Kevin J. Boyd.